GEOFLUIDS
Geofluids (2013) 13, 381–394 doi: 10.1111/gfl.12033

The sources and formation processes of brines from the Lunnan Ordovician paleokarst reservoir, Tarim Basin, northwest China

J. CHEN[1,2], D. LIU[1], P. PENG[1], C. YU[1], B. ZHANG[3] AND Z. XIAO[3]

[1]*State Key Laboratory of Organic Geochemistry, Guangzhou Institute of Geochemistry, Chinese Academy of Sciences, Guangzhou, China;* [2]*Graduate School of Chinese Academy of Sciences, Beijing, China;* [3]*Tarim Oilfield Company, PetroChina, Kuerle, China*

ABSTRACT

The most important petroleum exploration target in the Tarim Basin, northwest China, is the paleokarst reservoir. To understand the source and evolution of brine in this type of reservoir, a total of 37 formation-water samples were collected from the Middle-Lower Ordovician paleokarst reservoir in the Lunnan oilfield. The δD-$\delta^{18}O$ correlation and Cl/Br ratios reflect the mixture of two fluids: meteoric water and evaporated seawater. The different degree of mixture divided samples into two groups. Group 1 samples, from deep strata (5150–6667 m.b.s.l.) in the east of the field, with elevated δD (−53.5 to −38.0), $\delta^{18}O$ values (0.66–5.99), and lower Cl/Br ratios (336–478 for Cl/Br, except LN634-1 and LN631-1) were formed by evaporation of seawater plus a small contribution from meteoric water. Group 2 samples, from shallow strata (5038–6067 m.b.s.l.), in the west of the field, have contrasting features (−59.6 to −48.5 for δD, −0.47 to 2.17 for $\delta^{18}O$, and 501 to 871 for Cl/Br), which reflect a mixture of evaporated seawater with a high proportion of meteoric water. Both of the fluid types exchanged oxygen isotope with minerals. The investigation into cation composition reveals that, before entering into the current reservoir, waters suffered albitization of plagioclase; moreover, meteoric water dissolved evaporites and seawater experienced dolomitization. A mixing trend showed by strontium isotopes (0.709801–0.711628) gave further evidence for the mixture of two fluid types. Based on the correlation of geological history with our data, two infiltration models of meteoric waters can be constructed. According to the chemical and isotopic compositions of the waters, an east fluid regime (Group 1) and a west fluid regime (Group 2) have thus been defined. Better understanding of the subsurface fluid movement patterns may be helpful for the local exploration.

Key words: evaporated seawaters, formation waters, meteoric waters, paleokarst reservoir, Tarim Basin

Received 20 March 2012; accepted 11 March 2013

Corresponding author: Ping'an Peng, Guangzhou Institute of Geochemistry, Chinese Academy of Sciences, No. 511 Kehua Street, Guangzhou 510640, China.
Email: Pinganp@gig.ac.cn. Tel: 86 020 85290126. Fax: 86 020 85290117.

Geofluids (2013) **13**, 381–394

INTRODUCTION

Numerous studies have been carried out with the goal of understanding formation waters in oil fields (Clayton *et al.* 1966; Rittenhouse 1967; Collins 1975; Carothers & Kharaka 1978; Chaudhuri 1978). The results show that the chemical and isotopic composition of formation waters may provide insight into the sources, migration pathways, and water–rock interactions of brines over geological time. Such information can be helpful in interpreting petroleum sources and migration directions and in studying their effects on oil and gas such as biodegradation and thermochemical reduction. The quality of a reservoir, especially carbonate, can be substantially altered by water–rock interactions, which lead to mineral dissolution or precipitation. In addition, the spatial variation of brine compositions in oilfields may yield information about hydraulic compartmentalization and connectivity between production wells (e.g., Chaudhuri *et al.* 1987; Birkle *et al.* 2009), which is sometimes hard to obtain by other techniques.

Of all the recently found types of hydrocarbon reservoir in the Tarim Basin, for example, paleokarst, Paleozoic reef flat, Mesozoic delta, and Tertiary alluvial fan/flood plain (Yang & Sun 1999; Wang 2001; Ruan *et al.* 2009), the

paleokarst carbonate reservoir is becoming increasingly important. The Lunnan paleokarst reservoir is known for its high permeability and porosity but also has a high degree of heterogeneity across the whole reservoir. The permeability and porosity can reach as high as 748 mD and 18.79%, respectively, but average values are 0.3 mD and 1.22% (Yang & Han 2007). Although karstification is commonly found in carbonates worldwide (Mazzullo & Chilingarian 1996; Loucks 1999), formation water from deeply buried karst reservoirs has been poorly investigated. Many oilfield waters from carbonate reservoirs in previous studies were collected from shelf facies (e.g., limestones between the Pennsylvanian and early Permian in the Permian Basin, Stueber *et al.* 1998) or reef facies (e.g., Silurian strata in the Illinois Basin, Stueber & Walter 1991). The distinct characteristics of cave-hole-fissure structures in karst reservoirs may control water migration and water–rock interaction and be different from those of the hole-fissure structure in shelf and reef deposition.

Recently, many karst oilfields, including Hetianhe oil and gas field, Tazhong oilfield, and Tabei oilfields, have been found in the Tarim Basin (Fig. 1). During oil production, a high water content in the oil is typically encountered, which makes oil recovery inefficient. Take the Lunnan oilfield as an example; most of our samples (31 of 37 samples) have water contents higher than 50%. To enable further exploration and better production, it is necessary to study the sources and formation processes of these waters.

In the present study, we collected formation waters from 37 oil and gas wells. The waters had been produced from the Middle-Lower Ordovician paleokarst reservoir in the Lunnan oilfield, Tarim Basin. The chemical and isotopic compositions of the formation waters were analyzed. Our aims were (i) to trace the origin and evolution of oilfield waters in a typical paleokarst reservoir, (ii) to differentiate fluid regimes, based on the spatial distribution of geochemical properties, and (iii) to define possible permeability barriers.

GEOLOGICAL SETTINGS

The Lunnan oilfield, also known as the Lunnan Low Uplift, is located at the center of the Tabei Uplift, in the northern part of Tarim Basin (Fig. 1A). It is surrounded by the Luntai Uplift, Caohu Sag, Manjiaer Depression, and Halahatang Depression. It is one of the major petroleum production areas in the Tarim Basin. The range of heavy, normal, waxy, condensate oils and natural gases are produced from the Ordovician carbonate reservoir and the

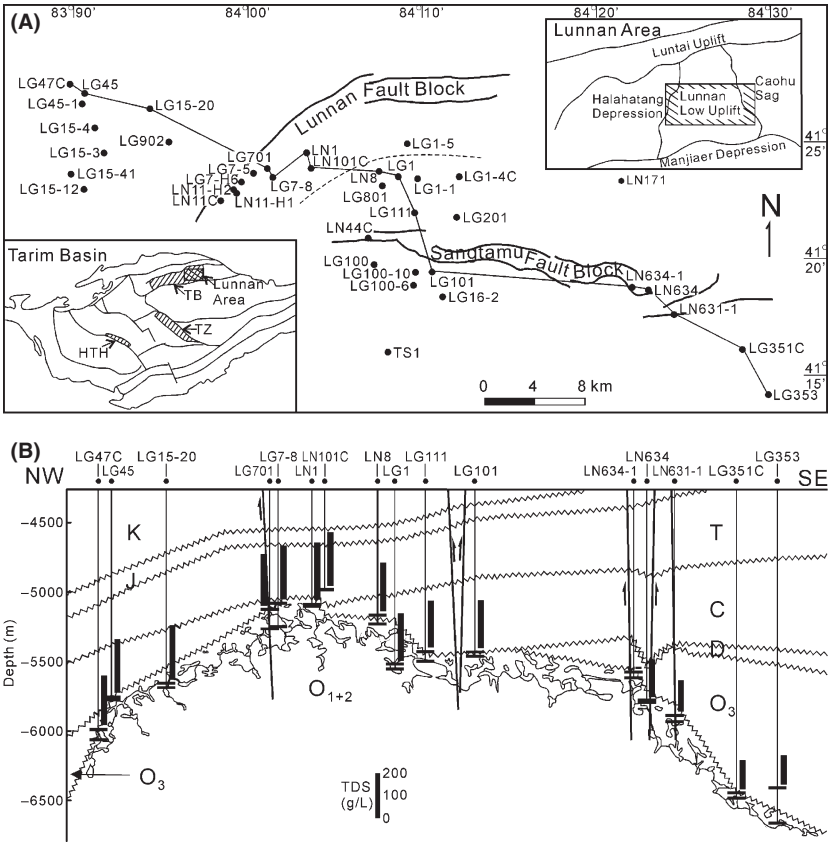

Fig. 1. (A) Study area and location of sampling wells (filled circles) in the Lunnan oilfield, Tarim Basin, China. Two groups dicsussed in article are divided by dashed line. Inset in Fig. A is structure map of Tarim Basin and Lunnan Area. Note that paleokarst Ordovician oilfields, including the Hetianhe oil and gas field (HTH), Tazhong oilfield (TZ) and groups of oilfields in the Tabei Uplift (TB) are shown in shaded area; (B) Strata profile from Well LG47C to Well LG353 (please see a line in Fig. A). TDS are showed in short filled columns.

Carboniferous, Triassic, and Jurassic clastic reservoirs in the Lunnan oilfield (Lu *et al.* 2004; Yang & Han 2007).

The depositional environments of the Lunnan oilfield can be divided into marine, transitional, and continental types, of ages ranging from Cambrian to Quaternary (Fig. 2). The Paleozoic section of the Lunnan oilfield is mainly composed of marine carbonate. Carboniferous and Permian sequences are marine to nonmarine transgressive–regressive successions, whereas sequences after the Triassic are nonmarine. Bedded evaporite minerals are not well recorded in the Lunnan Low Uplift, with only minor amounts of anhydrite found in Carboniferous and Paleogene strata (Pang *et al.* 2007; Xu & Ai 2011). Moreover, large amounts of bedded evaporites are widely deposited in the early and middle Cambrian strata (Tang *et al.* 2004).

The tectonic evolution of the Lunnan oilfield can be divided into four periods (Peng 2004). During the late Caledonian orogeny (early Paleozoic period), a north updip, nose-like structure was formed on a base of Precambrian metamorphic rock. Later, during the early Hercynian orogeny (late Paleozoic period), the nose-like structure was uplifted and became a NE–SW trending anticline. At the top of the anticline, Upper Ordovician, Silurian, and Devonian strata were completely eroded. During the late Hercynian and Indo-Chinese orogenies (late Paleozoic to early Mesozoic), another intense uplift removed the whole Permian and Upper Carboniferous strata on the top of the

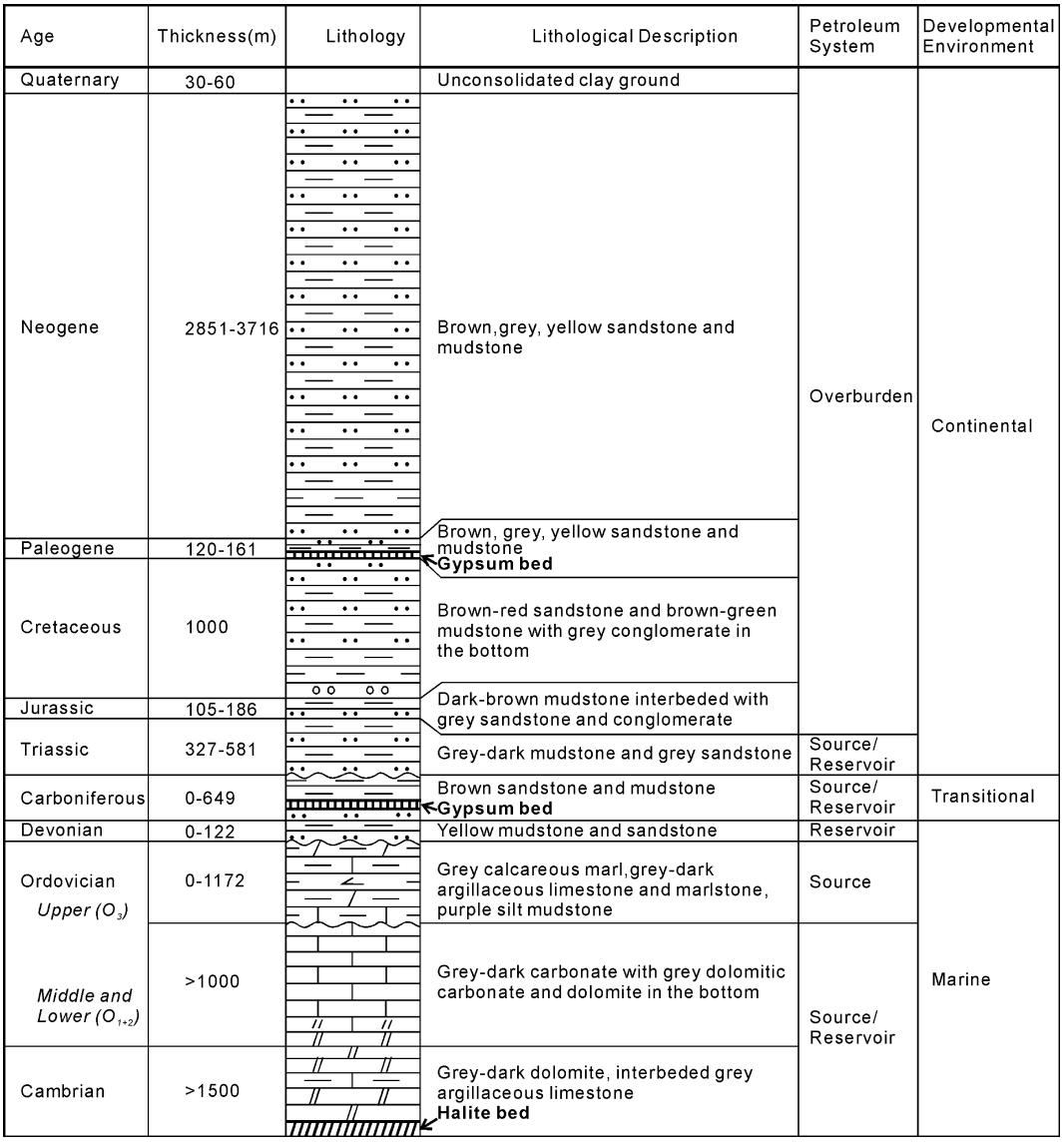

Fig. 2. Stratigraphic column of the Lunnan oilfield, Tarim Basin, China, adopted from Xiao *et al.* (2005), Gong *et al.* (2007) and Pang *et al.* (2007). Note halite bed in Cambrian strata and gypsum bed in Carboniferous and Paleogene strata.

anticline, and Middle-Lower Ordovician strata suffered meteoric leaching again. During the Yanshanian and Himalayan orogenies (late Mesozoic to Cenozoic), large amounts of clastic sediments were deposited following a long period of subsidence. At the same time, the Lunnan burial hill was formed following the depression of the north updip area of the Lunnan Uplift.

During two periods of exposures at the surface, the top of Middle-Lower Ordovician carbonate strata evolved into a karst system. It is commonly believed that the effective reservoir space is within the upper 200–300 m of Middle-Lower Ordovician paleokarst, which was governed by infiltration of meteoric waters (Gu 1999; Pang & Shi 2008). It is considered that karstification played an important role in the creation of caves and underground flow pathways, but the connectivity of Middle-Lower Ordovician reservoir space is low. This is responsible for the tilted oil–water boundary with different kinds of hydrocarbons occurring in the same region (Han *et al.* 2006; Pang *et al.* 2007).

There are two end-member types of oil in the Lunnan oilfield. One is heavy oil from the southwest side, generated from Ordovician source rocks in the northern Manjiaer Depression (Zhang *et al.* 2000; Wang *et al.* 2004; Xiao *et al.* 2005). The other is light oil from the southeast side, possibly from Cambrian-Lower Ordovician source rocks in Caohu Sag (Yang & Han 2007; Wang & Zhang 2008). The mixture of the two oils produced a wax-prone oil in the middle portion of the Lunnan oilfield (Lu *et al.* 2004).

SAMPLES AND METHODS

Except for one sample from the Triassic reservoir, all samples were collected from the paleokarst reservoir on the top of Middle-Lower Ordovician carbonate strata but from a range of depths, between 5000 and 6700 m below sea level (m.b.s.l., Fig. 1B). Ordovician samples fall into this typical karst interval (within the upper 300 m of Middle-Lower Ordovician reservoir), except for one sample, LG1, which is from a slightly deeper interval (within the upper 320–360 m).

Oilfield waters were sampled from production wells between July 2009 and September 2010. Two samples (LN634-1 and LN631-1) from gas wells in the east have high gas/water ratios, reaching 45 600 and 7170 m^3 per m^3, respectively, whereas others show low gas/water ratios (<900 m^3 per m^3). Artificial contamination did not take place because selected wells had not previously been water-injected for at least 6 months before sampling. Three water samples (LG45-1, LG15-41, and LG353) were collected even though the wells had undergone water injection <6 months before sampling. Despite the earlier injection history, these wells gave normal chemical and isotopic signatures that were similar to those of adjacent wells. The sample locations and the chemical and isotopic composition data are shown in Fig. 1A and Table 1, respectively.

The pH of the water samples was determined in the field. Alkalinities were measured by the H_2SO_4 titration method using a TitroLine Easy Schott automatic titrator (Lico *et al.* 1982). Samples of 50-ml volume were titrated to a pH of 2.5 with 0.05 N H_2SO_4 solutions, and the alkalinities were calculated from the amounts of acid used to reach the inflection points in the titration curves.

Total dissolved solids (TDS) were measured by the gravimetric method according to Clescerl *et al.* (1999). After filtration with a 0.45-μm filter, 0.5-ml samples of the brines were dried at 180°C until a constant weight was reached.

The anions were measured by ion chromatography following appropriate dilution (5000 times for Cl and 1000 times for Br and SO_4) with a Dionex ICS900 instrument with an AS19 ion-exchange column. The analytical precisions were better than 0.8% for Cl, 1.3% for Br, and 4.3% for SO_4. The major cations in the diluted solutions (5000 times for all cations) were analyzed with a Varian Vista-Pro inductively coupled plasma-optical emission spectrometer (ICP-OES) with an analytical precision of better than 5%.

The $\delta^{18}O$ and δD isotopic compositions were determined by the gaseous equilibration method using a GV IsoPrime II isotope ratio mass spectrometer coupled with a Dual Inlet and an online aqueous preparation system (Multiprep). The $\delta^{18}O$ and δD isotope values are reported relative to Vienna Standard Mean Ocean Water (V-SMOW). Replicated analyses yielded a precision of ± 0.08 and ± 1.5 for $\delta^{18}O$ and δD, respectively. The equations of Sofer & Gat (1972) and Horita (2005) were used to correct the ^{18}O and D activity data for the isotope salt effects.

The $^{87}Sr/^{86}Sr$ ratios in the formation waters were determined by TRITON TIMS after the strontium was extracted with a Sr-Spec ion-exchange resin. All measured $^{86}Sr/^{88}Sr$ values were fractionation-corrected to $^{86}Sr/^{88}Sr = 0.1194$. The measurement of the $^{87}Sr/^{86}Sr$ value of the NBS987 (National Bureau of Standards) standard was 0.710254 ± 4 (2σ, $n = 14$).

RESULTS

The chemical and isotopic compositions of formation water from the Lunnan karst reservoir are summarized in Table 1.

The charge balances of the samples are <5% (Table 1). The samples have a pH between 5.96 and 6.96 except for one (LN44C) that has a low pH of 3.50. The TDS are between 129 and 259 g l^{-1}, except for the value of 9.82 g l^{-1} in LN634-1, from a gas well. Based on the salinity classification (Davis 1964), 36 waters are brines, while LN634-1 is a brackish water. The abnormally low salinity of water from LN634-1 could be due to the

Table 1 Chemical and isotopic composition of formation-water samples in the Lunnan oilfield, Tarim Basin, China.

Well	Group	Age	Internal depth (m)	Water fraction (%)	Temperature on wellhead (°C)	pH	TDS (g l^{-1})	Alkalinity (mg l^{-1})	Cl (mg l^{-1})	Br (mg l^{-1})	SO_4 (mg l^{-1})	Na (mg l^{-1})	Ca (mg l^{-1})	Mg (mg l^{-1})	K (mg l^{-1})	Sr (mg l^{-1})	Ba (mg l^{-1})	Charge Balance (%)	$\delta^{18}O$ V-SMOW	δD V-SMOW	$^{87}Sr/^{86}Sr$
LG47C	2	O_{1+2}	5993–6067	68.2	35	6.67	220	175	124 500	185	525	69 000	11 500	842	1460	436	6.90	2.35	0.35	−56.0	0.711173
LG45	2	O_{1+2}	5763.2–5770	83.6	52	6.52	240	n.m.	136 500	210	532	78 900	11 400	951	1990	526	7.30	3.58	1.42	−57.5	0.711164
LG45-1	2	O_{1+2}	5748.1–5762	83.0	28	6.39	236	104.	138 500	212	291	73 600	10 700	894	2070	461	11.0	−0.49	2.17	−58.1	n.m.
LG15-4	2	O_{1+2}	5751–5809	47.8	43	n.m.	234	n.m.	135 400	270	307	72 600	11 400	907	1790	485	12.1	0.39	1.72	−54.1	n.m.
LG15-41	2	O_{1+2}	5732–5759	100	26	6.23	245	n.m.	137 100	242	312	69 800	11 200	926	1420	484	18.4	−2.06	0.98	−48.5	n.m.
LG15-12	2	O_{1+2}	5702–5817	77.9	52	6.07	252	n.m.	142 900	225	744	76 300	12 000	940	2020	494	7.50	0.17	0.54	−59.6	0.710670
LG15-3	2	O_{1+2}	5701.1–5718	95.1	46	6.36	259	n.m.	145 900	219	254	81 100	12 100	924	1980	487	16.3	1.85	1.63	−58.9	n.m.
LG15-20	2	O_{1+2}	5657.5–5681	59.5	35	n.m.	244	n.m.	140 400	263	297	75 200	11 200	852	1710	489	8.10	−0.12	1.45	−50.5	n.m.
LG902	2	O_{1+2}	5579.5–5630	73.3	40	6.33	253	91.4	153 100	211	282	78 600	11 700	940	1890	501	13.3	−2.16	1.89	−53.3	n.m.
LN11C	2	O_{1+2}	5318.9–5817	49.4	47	6.42	251	n.m.	144 000	253	312	79 500	11 800	991	1790	496	14.9	1.44	1.86	−53.0	n.m.
LN11-H2	2	O_{1+2}	5240.3–5595	60.6	51	6.96	241	n.m.	138 000	190	462	74 800	12 000	1080	1230	603	2.70	1.10	0.45	−57.5	0.710776
LN11-H1	2	O_{1+2}	5209.5–5530	31.5	35	6.39	244	88.5	151 200	235	420	76 600	11 700	1030	1270	572	7.30	−2.72	0.96	−51.6	n.m.
LG7-H6	2	O_{1+2}	5196–5651	50.8	58	6.53	243	n.m.	134 900	171	291	73 500	12 000	1090	1210	626	6.70	1.62	−0.28	−57.9	0.710806
LG7-5	2	O_{1+2}	5245–5270	85.4	85	6.17	248	76.3	133 700	223	201	73 500	11 400	974	1720	500	4.20	1.70	1.32	−52.0	0.710541
LG701	2	O_{1+2}	5121.2–5262.5	80.4	45	6.87	230	86.7	132 300	198	211	74 100	11 300	1000	1560	556	4.40	2.41	1.03	−57.6	0.710673
LG7-8	2	O_{1+2}	5078.5–5250	34.8	52	6.76	240	n.m.	138 000	159	264	76 400	12 400	1110	1150	646	8.80	2.30	−0.47	−57.4	0.710863
LN1	2	O_{1+2}	5038–5052	100	17	6.18	255	n.m.	133 900	171	333	74 800	11 800	1020	1260	546	4.00	2.51	0.45	−57.5	0.710847
LN101C		T	4984–4984.5	92.8	65	6.09	239	n.m.	134 500	117	338	74 200	11 900	900	1060	300	3.50	1.73	−2.49	−57.9	0.710303
LG1-5	2	O_{1+2}	5108.9–5180	89.6	75	6.34	226	54.9	132 200	191	233	72 700	11 400	1080	1260	498	5.00	1.75	1.32	−51.9	0.710795
LN8	1	O_{1+2}	5167.2–5231.4	57.6	19	6.43	217	114	119 200	321	104	60 600	11 700	1020	1560	520	17.8	−0.15	2.50	−49.5	n.m.
LG801	1	O_{1+2}+C	5150.6–5218	97.7	30	6.03	228	68.8	121 600	310	81.0	63 300	11 800	1020	1660	526	39.0	0.68	2.48	−49.5	n.m.
LG1	1	O_{1+2}	5520–5555	95.5	78	6.66	212	69.4	123 000	274	35.0	67 200	12 000	1040	1980	542	21.8	2.86	1.61	−48.2	0.710430
LG1-1	1	O_{1+2}	5211.9–5249.6	80.1	32	6.42	210	110	126 900	326	165	58 600	12 100	1050	1440	569	40.4	−4.21	2.55	−43.4	n.m.
LG1-4C	1	O_{1+2}	5444–5510	90.4	20	6.26	180	97.7	100 800	245	57.8	47 000	13 700	1040	1260	642	17.5	0.30	0.66	−46.5	0.711628
LG111	1	O_{1+2}	5429.5–5500	81.4	56	6.65	209	69.4	120 800	273	17.6	65 200	12 300	1070	2160	535	48.1	2.86	2.19	−46.5	0.710311
LG201	1	O_{1+2}+C	5350–5358	98.6	45	6.26	207	72.3	118 100	337	81.8	55 700	12 800	1030	1670	567	30.5	−1.98	2.75	−47.5	n.m.
LN44C	1	O_{1+2}	5301.3–5433	86.8	37	3.50	232	n.m.	126 100	331	132	62 000	11 000	1030	2020	503	40.8	−2.38	2.58	−43.3	n.m.
LG100	1	O_{1+2}	5431.2–5525	93.9	38	6.26	230	78.7	118 000	340	78.0	63 400	12 000	983	1940	521	24.4	2.53	2.61	−42.5	n.m.
LG100-10	1	O_{1+2}	5412.4–5442	98.5	54	6.35	244	66.5	131 800	339	157	68 800	11 600	964	2280	461	11.6	0.01	3.05	−52.3	n.m.
LG100-6	1	O_{1+2}	5433.5–5475	80.9	46	6.90	219	66.5	121 600	268	102	63 700	11 800	1010	2100	487	10.3	1.10	1.74	−53.0	0.710074
LG101	1	O_{1+2}	5432–5462	98.6	39	6.31	215	91.4	121 700	255	80.4	65 900	11 800	973	1880	480	11.8	2.26	1.42	−53.5	0.710188
LG16-2	1	O_{1+2}	5478–5505	96.1	42	6.93	223	61.9	126 400	268	99.3	67 100	11 100	941	2230	438	13.4	0.75	1.46	−53.5	0.709995
LN171	1	O_{1+2}	5443.5–5475	90.2	32	6.17	222	n.m.	113 500	295	139	55 500	11 700	1010	1700	517	42.4	−1.06	1.64	−46.6	n.m.
LN634-1	1	O_{1+2}	5578–5618.5	24.6	22	5.96	9.82	n.m.	3786	3.20	169	1370	994	47.3	57.5	8.10	1.80	2.14	−5.25	−58.6	0.710359
LN634	1	O_{1+2}	5780–5796	50.9	40	6.62	167	120.	94 840	261	5.80	50 400	7870	701	2670	343	142	0.82	4.70	−41.4	0.709801
LN631-1	1	O_{1+2}	5891–5936	20.5	23	6.85	141	n.m.	72 640	114	1100	25 000	17 300	838	1380	192	7.60	−0.24	−1.41	−53.1	0.709820
LG351C	1	O_{1+2}	6448.5–6486.5	89.5	90	6.71	129	232.	75 070	205	83.0	41 200	5590	481	2120	289	249	1.26	5.52	−38.0	0.710120
LG353	1	O_{1+3}	6411.7–6667	84.3	47	6.30	131	150.	74 350	222	35.0	39 000	6040	493	2320	294	25.8	0.17	5.99	−42.7	0.709935

Water content (%) = water volume/(water volume+oil volume)·100.Charge balance (%) = $(\sum Z \cdot m_c - \sum Z \cdot m_a)/(\sum Z \cdot m_c + \sum Z \cdot m_a) \cdot 100$; Z is ion's charge, m_c and m_a are molalities of the cationic and anionic species, respectively.

dilution of condensed water vapor (aqueous condensate). Another sample, from gas well LN631-1, has a normal salinity (141 g l^{-1}), possibly due to its relatively small gas/water ratio (7170 m^3 per m^3) and only a small dilution by condensed water vapor. Generally, samples from the west region show higher TDS than samples from the east region (Fig. 1B).

The cation and anion concentrations of the samples are also listed in Table 1. The predominant ions are Cl and Na. Except for LN634-1, Cl and Na concentrations range from 72 640 to 153 100 and 25 000 to 81 100 mg l^{-1}, respectively. When the ion concentrations are plotted on a Piper diagram, all waters are defined as Cl-Na type, although two samples from gas wells (LN634-1 and LN631-1) have higher Ca contents. The concentrations of their anions (Br, SO_4, and HCO_3) are much lower than that of Cl (Table 1). The concentrations of Ca, the second most predominant cation, range from 17 300 to 13 700 mg l^{-1} except for that of LN634-1. In terms of the ratio $mCa/(mSO_4 + 1/2mHCO_3)>1$, we may also classify our samples as Na–Ca–Cl type for special geological attention. The other major cations are K, Mg, Sr, Ba, etc., which are commonly reported in other oilfield waters (e.g., Egeberg & Aagaard 1989; Stueber *et al.* 1993; Cai *et al.* 2001).

The δD values of the Middle-Lower Ordovician samples show negative values between −58.6 and −38.0, while the $\delta^{18}O$ values are mostly positive, ranging from −0.47 to 5.99, except for those of LN631-1 (−1.41) and LN634-1 (−5.25). These data differentiate the samples from seawater and local meteoric water, as shown in Fig. 3. Negative δD values imply an important contribution of meteoric water to formation water.

The isotopic compositions of Sr were also measured. The $^{87}Sr/^{86}Sr$ ratios range from 0.711628 to 0.709801, higher than those of seawaters of any geological time (<0.7091, Burke *et al.* 1982). The addition of an additional contribution of radiogenic ^{87}Sr from nonmarine sources should thus be considered.

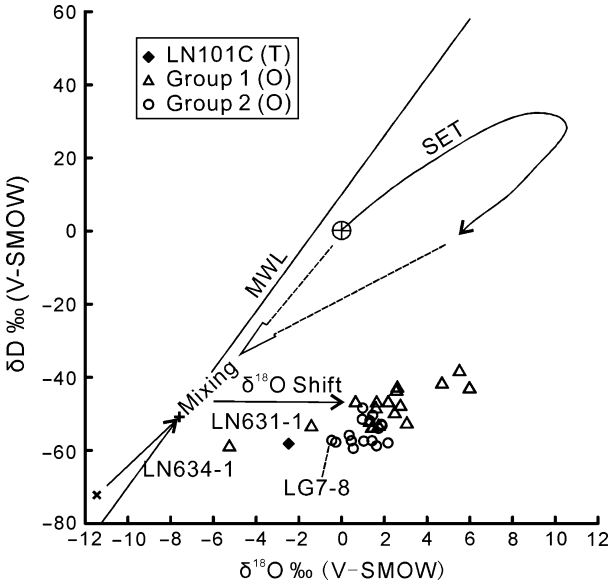

Fig. 3. Hydrogen-oxygen isotopic relationship of formation waters. Meteoric water line (MWL) is from Craig (1961) and seawater evaporation trajectory (SET) is from Holser (1979), quoted as Stueber & Walter (1991). X symbol is local Kongque River water (δD = −72‰, $\delta^{18}O$ = −11.5‰) from Cai *et al.* (2001). + symbol is calculated paleometeroic water (δD = −51.4‰, $\delta^{18}O$ = −7.67‰, see text for details).

DISCUSSION

Water origin and water–rock interaction as indicated by oxygen and hydrogen isotopic ratios

The ^{18}O-D isotopic relationship is illustrated in Fig. 3. It seems that the formation waters do not have a single origin but are possibly mixtures of seawater and meteoric water because all the data fall away from the seawater point and the meteoric water line. Formation waters that are mixtures of seawater and meteoric water are common in sedimentary basins (e.g., Illinois Basin, Stueber & Walter 1991).

Strong water–rock interaction may cause a positive ^{18}O shift and keep the D isotopic composition of basin brines unchanged (Clayton *et al.* 1966; Kharaka & Thordsen 1992). This interpretation is supported by the occurrence of water at depths below 5000 m and the elevated temperature in the Ordovician reservoir (>118°C, based on a local thermal gradient of 1.97°C per 100 m, Fan & Zhou 1990).

Considering the negative δD of all the formation waters, we consider that the contribution of meteoric water is important even though the proportion is unknown at present. We conclude that it is highly unlikely that seawater will give rise to hydrogen isotopic values <−40 by geological processes.

Based on the $\delta^{18}O$-δD relationship and the sampling locations, the formation waters can be roughly divided into two groups. Group 1 is located on the east side of the Lunnan Uplift at greater depths (5167–6667 m.b.s.l.). Samples are enriched in ^{18}O and D, except those from LN631-1 and LN634-1, which are influenced by water condensation as shown by abnormally low isotope composition values. High δD values (−53.5 to −38.0) in Group 1 reflect possible mixing with more evaporated seawater, while heavy $\delta^{18}O$ values (0.66–5.99) indicate stronger water–rock interaction. Group 2, containing the samples from the west side of the Lunnan Uplift at a shallower depth (5038–5871 m.b.s.l.), shows lower $\delta^{18}O$ (−0.47 to 2.17) and δD (−59.6 to −48.5) values relative to samples from the east side (Fig. 3). This feature demonstrates that they received a larger contribution from meteoric waters

and underwent less water–rock interaction. The lightest $\delta^{18}O$ and δD values are from two of the shallowest samples: Triassic well LN101C (4984–4984.5 m.b.s.l., $\delta^{18}O = -2.49$; $\delta D = -58.0$) and Ordovician well LG7-8 (5078.5–5250 m.b.s.l., $\delta^{18}O = -0.47$; $\delta D = -57.4$). Thus, the area near LG7-8 is the most likely pathway for meteoric waters.

According to the geological history of this region, one of the most likely origins of meteoric waters is paleometeoric waters that infiltrate long after the Tarim Basin ended its marine deposition. The sedimentological evidence shows that the late Hercynian and Indo-Chinese orogenies turned the Tarim Basin from a marine to a continental setting and provided a suitable condition for meteoric water to infiltrate the Ordovician reservoir. At that time, the latitude of the Tarim Block reached −35.7°N (Fan & Ma 1990), which is lower than the present-day latitude of −40.0°N. The latitude effect on meteoric water can introduce an increase of $\delta^{18}O$ by 0.6 per degree of latitude decrease (Mook 2000). Not considering other effects on meteoric water, calculated $\delta^{18}O$ and δD values of −7.67 and −51.4 for paleometeoric water can be assumed to represent the isotopic composition of the meteoric end member (Fig. 3).

Another possible origin of the meteoric waters is that Quaternary meteoric waters might have infiltrated as implied by the samples' good linear relationship with the modern meteoric waters, even though the reservoir is located 5000 m underground. Young meteoric waters were found in some deep reservoirs in the Gulf of Mexico by Birkle *et al.* (2002) and Birkle & Maruri (2003). After determining the residence time of the formation waters by the ^{14}C method, they suggested that brines in the Activo Samaria-Sitio Grande reservoir (3500–4500 m.b.s.l.) and the Activo Lunna reservoir (5000–6000 m.b.s.l.) consisted of meteoric water and evaporated seawater that had infiltrated no earlier than the late Pleistocene period. Therefore, Quaternary meteoric waters are invoked as another possible origin. Unfortunately, no age dating was performed on the Middle-Lower Ordovician formation waters, so it is not possible to discount a Quaternary meteoric water origin.

Solute origins and water–rock interactions

Cl-Br relationship

Neither chloride nor bromide participate in any diagenetic reactions with silicate, carbonate, sulfide, or sulfate rock-forming minerals in sedimentary basins, except for dissolution or precipitation of evaporite minerals; therefore, the Cl-Br relationship is a useful tool to study the origin of formation waters by comparing data with the seawater evaporation trajectory (SET for short; Hanor 1994; Worden 1996; Kharaka & Hanor 2007).

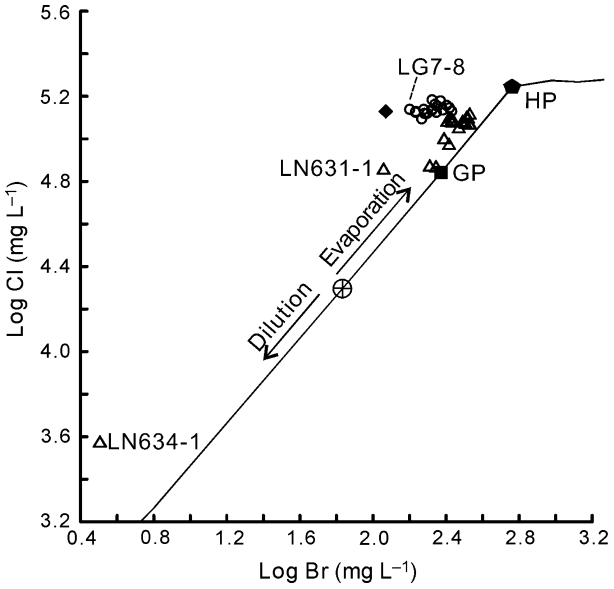

Fig. 4. Cl versus Br relationship of formation waters. The seawater evaporation trajectory is generated using data from Fontes & Matray (1993). GP means gypsum precipitaion. HP means halite precipitation. Sample symbols are defined in Fig. 3.

As shown in Fig. 4, all data are distributed on the left side of the SET, implying that the major anions resulted from halite dissolution and evaporation of seawater. Halite dissolution without recrystallization produces fluids with a higher Cl/Br ratio as only small amounts of bromide can be contained in the halite crystal when halite precipitates (Stoessell & Carpenter 1986; McCaffrey *et al.* 1987). Therefore, on the Cl-Br graph, evaporation of seawater will produce data on the SET, while halite dissolution will move the data away from the SET. Both processes affect our Middle-Lower Ordovician formation waters.

The two groups defined by the $\delta^{18}O$-δD relationship can be found in the Cl-Br relationship. Group 1 is almost sub-parallel to the SET, indicating less halite dissolution and a greater contribution of evaporated seawater salt (Cl/Br mass ratio = 336–478, slightly higher than the 291 value of seawater), with the exception of the gas wells LN634-1 and LN631-1, with abnormally high ratios (1183 and 637, respectively). Group 2 is remote from the SET, reflecting additional halite dissolution (501–871) besides evaporated seawater. Sample LG7-8 shows the highest Cl/Br ratio (871) in the Ordovician reservoir, while LN101C shows the highest Cl/Br ratio (1150) of all. Considering that they are at the shallowest locations with the lightest $\delta^{18}O$ and δD values, we speculate that formation water that dissolved halite descended from the overlying strata into the Ordovician reservoir through the LG7-8 region and migrated into other districts.

However, evaporite minerals are not abundant in all Lunnan stratigraphic sequences. Minor amounts of gypsum are

found in the Kalashayi Formation mudstone in the Lower Carboniferous strata. According to Xu & Ai (2011), the Kalashayi Formation mudstone was deposited in a limited lagoon-face environment. It is possible that the fluids dissolved all the halite occluded in the Kalashayi Formation mudstone, left gypsum as a remnant, and then intruded into the underlying Ordovician reservoir. A similar example is found in formation water from Mississippian–Pennsylvanian reservoirs in the Illinois Basin (Stueber *et al.* 1993). These authors suggested that formation waters affected by halite dissolution derived from the evaporite zone in the St. Louis Limestone, which now only contains gypsum. Historical presence of salts can be inferred from bedded halite, with a thickness of 115–225 m in Lower Carboniferous strata in the adjacent Tahe oilfield, south of the Lunnan oilfield (Zhou *et al.* 1999). Based on the geological history, the Tahe oilfield is in the downdip area of the Tabei Uplift. Therefore, Lower Carboniferous strata, including bedded halite, could have been retained in the Tahe oilfield when it was eroded at the top of the anticline in the Lunnan Area. Another possibility is the lacustrine gypsum evaporites in Paleogene strata that are widely reported for the Tarim Basin.

Drilling shows that the Cambrian strata contain significant amounts of evaporite minerals in some regions of the Tarim Basin (Tang *et al.* 2004). Some researchers have described the possibility of upward, cross-formational fluids migrating from the underlying strata to the Ordovician reservoir in the Tazhong oilfield (Cai *et al.* 2001) and in the Tahe oilfield of the Tarim Basin (Li *et al.* 2011). In the case of the Lunnan oilfield, wells have not penetrated into Cambrian strata. According to existing data from well TS1 (Fig. 1A), which pierced the Cambrian strata at about 1524 m depth, no halite was found (Yun & Zhai 2008). If upward-moving waters dissolving halite intruded from the deeper Cambrian bedded halite, wells near faults or the deepest well should show the highest Cl/Br ratios. The fact that the highest Cl/Br ratios were found in the shallowest wells, LN101C and LG7-8, eliminates this possibility.

As to the origin of the evaporated seawater, connate seawater is not applicable here. According to the geological history, meteoric water should have displaced Ordovician connate seawater during the subaerial exposure during the early Hercynian orogeny and later during the late Hercynian and Indo-Chinese orogenies. Evaporated seawater derived from other strata may have invaded here during the continual burial period after the Triassic epoch. As Group 1 in the east shows, deep strata are mainly evaporated seawaters, with a potential origin from marine carbonate strata of the Lower Ordovician and Cambrian in Caohu Sag in the east of the Lunnan oilfield.

Cation–Br relationships

Unlike chloride and bromide, cations in formation water can be strongly influenced by water–rock interactions (Kharaka & Hanor 2007). Based on cation–bromide relationships, we can identify the types of water–rock interactions that occurred. Comparing cations with the SET (Fig. 5), the Middle-Lower Ordovician formation water from the Lunnan oilfield shows an enrichment of Ca and Na, depletion of Mg, and variable K content. The compositional difference between the two groups mentioned above is also reflected in their cation–Br relationships.

The mean Mg/Br mass ratio of 4.39 in Ordovician samples yields an average depletion of 77% relative to that of seawater (19.4), while the mean Ca/Br mass ratio of 57.4 indicates a 9.29-fold enrichment relative to seawater (Fig. 5A,B). The main mechanism for Ca enrichment coupled with Mg depletion could be dolomitization of carbonates, widely reported by other researchers (e.g., Egeberg & Aagaard 1989; Stueber & Walter 1991). The Ca enrichment (485 meq l^{-1}) relative to seawater exceeds Mg depletion (304 meq l^{-1}) by about 59%, indicating that another mechanism is responsible for altering Ca–Mg relations, in addition to dolomitization. Gypsum dissolution during dissolution of evaporites by meteoric water might be a source of additional Ca.

Another mechanism for Ca enrichment in a fluid might be albitization of plagioclase, with an exchange of 2 Na ions for 1 Ca ion. This process has been described for sedimentary basins around the world (Davisson & Criss 1996). A Ca_{excess}-$Na_{deficit}$ plot is shown in Fig. 6, where the excess of Ca and the deficit of Na are defined as follows:

$$Ca_{excess} = (Ca_{meas} - (Ca/Cl)_{sw} \cdot Cl_{meas}) \cdot 2/40.08$$

$$Na_{deficit} = ((Na/Cl)_{sw} \cdot Cl_{meas} - Na_{meas}) \cdot 1/22.99$$

If evaporated seawaters were just altered by dolomitization and not by albitization of plagioclase, no linear relationship between Ca_{excess} and $Na_{deficit}$ would be found, which is in contrast to the good linear relationship for some samples from Group 1. Halite dissolution, as reflected in other samples, caused a shift from Na depletion to Na enrichment and changed the original signature of 1:2 Ca–Na exchange. Thus, albitization of plagioclase by 1:2 Ca–Na exchange is confirmed for the Middle-Lower Ordovician formation waters. It can be concluded that Mg depletion resulted completely from dolomitization, while Ca enrichment is derived from dolomitization, gypsum dissolution, and albitization of plagioclase. Excluding the results from LN634-1 and LN631-1, the greater enrichment of Ca (514 meq l^{-1}) and lesser depletion of Mg (259 meq l^{-1}) in Group 2 compared to Group 1 (460 and 381 meq l^{-1} for Ca enrichment and Mg depletion, respectively) suggest different mixing proportions of evaporated seawater salts and dissolution of evaporites.

In the Lunnan stratigraphic column, dolomitic carbonates and dolomites were present in the bottom of the

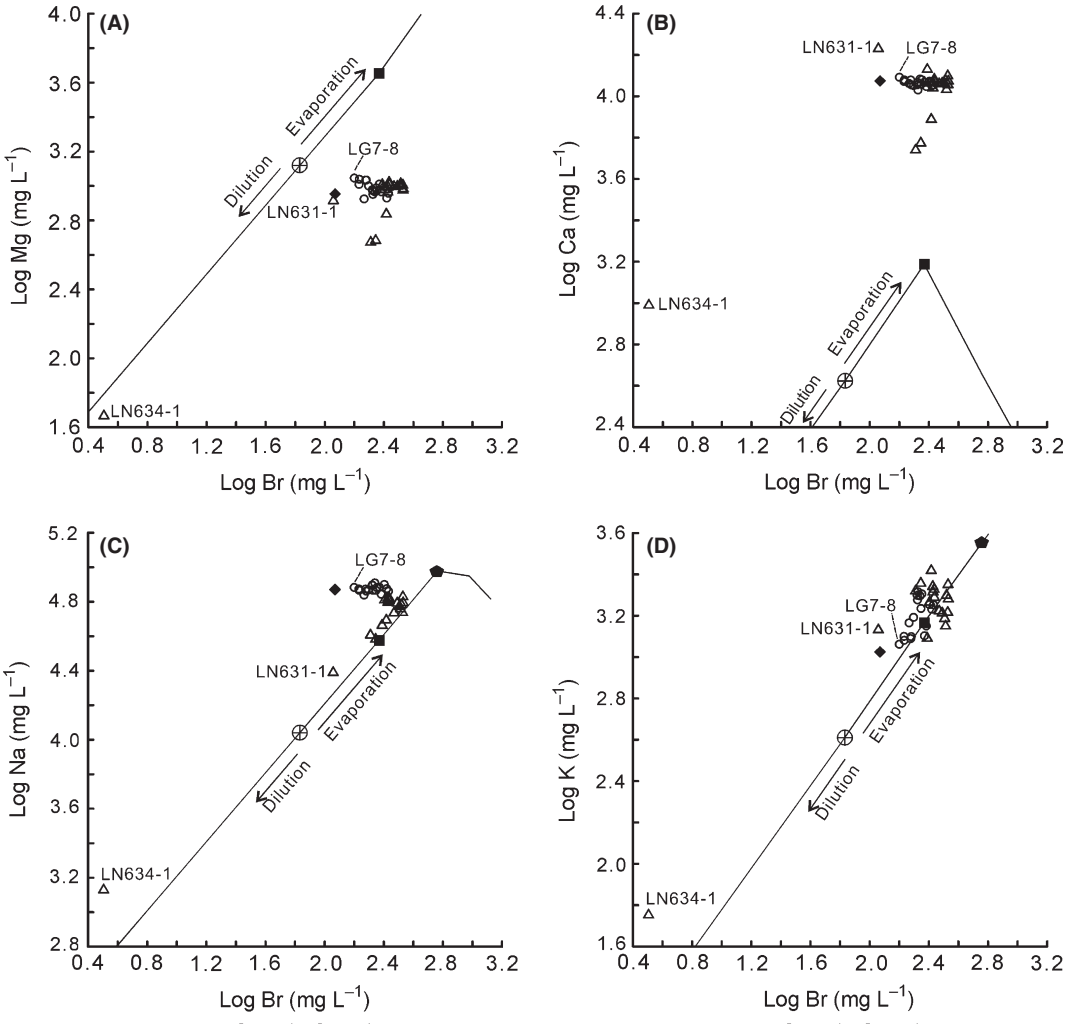

Fig. 5. Cations versus Br relationships of formation waters. (A) Mg versus Br; (B) Ca versus Br; (C) Na versus Br; (D) K versus Br. Symbols are defined in Figs 3 and 4.

Lower Ordovician strata, while extensive dolomites were found throughout the Cambrian strata (Fig. 2). Therefore, it is inferred that evaporated seawater altered by dolomitization was expelled upward to the top of the Middle-Lower Ordovician reservoir. Albite is not found in the Middle-Lower Ordovician carbonate strata or vein minerals, so the exchange of Ca and Na in all our samples implies that the reaction will have occurred in the underlying or overlying reservoir.

Our samples indicate Na enrichment by an average of 78%, as indicated by a mean Na/Br mass ratio of 287 compared to a seawater value of 162 (Fig. 5C). In sedimentary basins, the main water–rock interactions involving sodium are either albitization of plagioclase and K-feldspar or halite dissolution and precipitation (Davisson & Criss 1996). In the present case, although Ca is elevated by albitization, Na seems to be not measurably influenced by this reaction as so much Na is derived from halite dissolution that the loss of Na by albitization effectively cannot change Na concentration. The greater Na enrichment in Group 2 (123%) than that in Group 1 (35%) reconfirms the different roles of halite contribution.

The K contents of all samples, except LN634-1, are close to the SET, showing an average enrichment of 23%, while two samples in Group 2 and seven samples in Group 1 lie slightly below the SET, suggesting a depletion of K (Fig. 5D). However, in contrast to the other cations, K in Group 2 is sub-parallel to the SET, with the lowest K contents in LN101C (1060 mg l^{-1}) and LG7-8 (1150 mg l^{-1}), while K in Group 1 shows a larger variability near the SET. The lowest K contents, in LN101C and LG7-8, may be explained by infiltrating meteoric water with low K content from overlying strata.

SO_4-Br relationship

From the SO_4-Br relationship (Fig. 7), all samples except LN634-1 show a strong SO_4 depletion. Depletion in

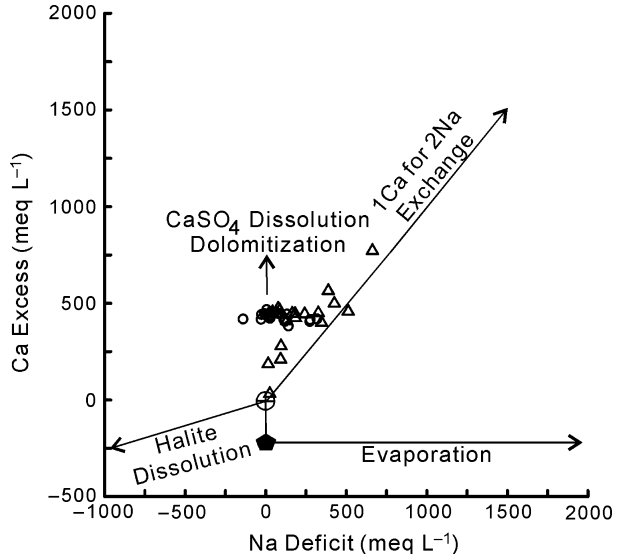

Fig. 6. Ca excess versus Na deficit in formation waters. Symbols are defined in Figs 3 and 4.

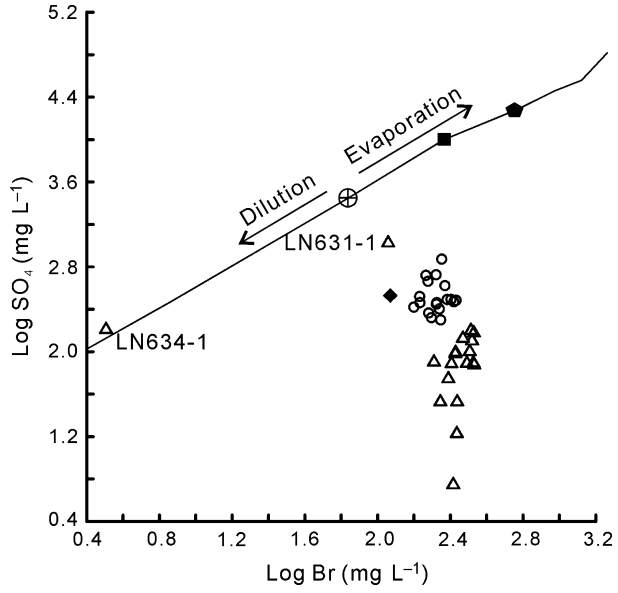

Fig. 7. SO4 versus Br relationship of formation waters. Symbols are defined in Figs 3 and 4.

Group 1 (99%) seems greater than Group 2 (96%). The depletion is commonly due to gypsum precipitation, which is often related to dolomitization of carbonates with an increase in Ca concentration. In addition, SO_4 depletion may be ascribed to thermochemical sulfate reduction (TSR) in the reservoir, or underlying and overlying strata. The reservoir temperature ranges from 118 to 149°C, which is high enough to initiate TSR (Machel 2001; Worden *et al.* 1995). However, there is no H_2S reported in gas reservoirs in this region, and we could not detect

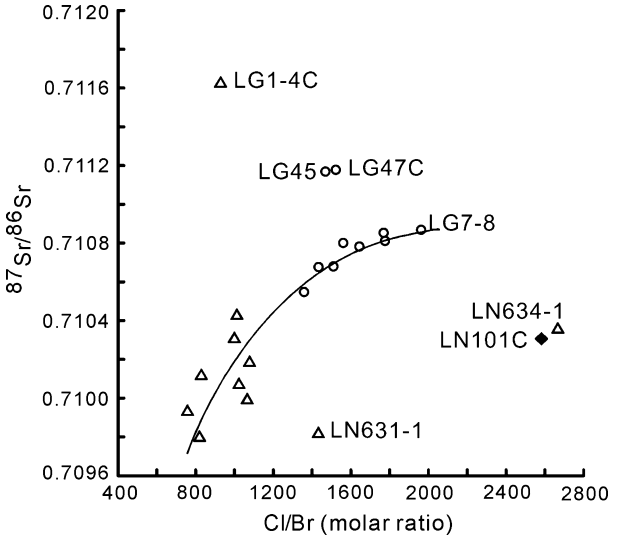

Fig. 8. $^{87}Sr/^{86}Sr$ ratios versus Cl/Br in formation waters. Symbols are defined in Figs 3 and 4.

aqueous HS^- in brines. Therefore, we conclude that TSR possibly occurred in underlying or overlying strata as one way to reduce aqueous SO_4.

$^{87}Sr/^{86}Sr$ isotope ratios

To trace the exotic interference (e.g., mixture of fluids, water–rock interaction), $^{87}Sr/^{86}Sr$ versus Cl/Br is plotted in Fig. 8. The $^{87}Sr/^{86}Sr$ ratios (0.709801–0.711628) are not only higher than values for Ordovician seawater (0.7078–0.7090), but also than those of marine water over all geological times (<0.7091, Burke *et al.* 1982). High $^{87}Sr/^{86}Sr$ ratios in formation waters can be attributed to the interaction with radiogenic minerals. In sedimentary basins, micas and K-feldspars in siliciclastic rocks and potash salts in evaporite minerals are enriched in radiogenic ^{87}Sr (e.g., Russell *et al.* 1988; Chaudhuri & Clauer 1993; Barnaby *et al.* 2004). Fluids interacting with these minerals will be characterized by high $^{87}Sr/^{86}Sr$ ratios.

Generally, samples in Group 2, from the west area, have higher Cl/Br and $^{87}Sr/^{86}Sr$ ratios than samples in Group 1, from the east area, with a few exceptions (LG1-4C, LN631-1, LN634-1; Fig. 8). The spatial distribution can be explained by mixing processes of ^{87}Sr-enriched meteoric water from overlying strata with relatively ^{87}Sr-depleted evaporated seawater from underlying strata. LG7-8 fluid shows a high $^{87}Sr/^{86}Sr$ ratio of 0.710862. It is located in a pathway of diagenetically altered meteoric water. However, sample LN101C shows an anomalously low $^{87}Sr/^{86}Sr$ ratio (0.710303).

Gypsum in evaporite minerals is considered to have the strontium isotope signature of contemporaneous seawater, as strontium is partly substituted for calcium in gypsum crystals. Meteoric waters dissolving evaporites (mainly

halite and possibly gypsum) will acquire the ^{87}Sr signature from contemporaneous seawater when gypsum is precipitated. However, the highly radiogenic signature in these Tarim samples excludes the possibility that the radiogenic ^{87}Sr was derived from gypsum dissolution. There is no evidence of potash salt deposits in the stratigraphic sequences here. The potential pathway of meteoric water in the shallowest well, LG7-8, shows that radiogenic ^{87}Sr was supplied by reactions with K-bearing minerals when meteoric waters penetrated into the subsurface. Extensive terrestrial mudstones and sandstones deposited after the Permian epoch provide abundant micas and K-feldspars. The negative correlation of ^{87}Sr versus K of most samples (samples in line in Fig. 7, $R^2 = 0.85$, not shown here) supports the speculation of higher $^{87}Sr/^{86}Sr$ signatures toward the end member of samples with a lower K content.

The reaction with K-bearing minerals in overlying strata may be accompanied by plagioclase albitization, which gives rise to concomitant Ca enrichment. Both reactions require feldspar-rich clastic rocks.

Other sources for strontium with low ^{87}Sr signature are evaporated seawaters from underlying marine strata and possibly strontium released from the dolomitization of carbonate, which also represents the strontium isotope signatures of underlying marine strata. This process would give rise to a $^{87}Sr/^{86}Sr$ ratio typical for the Lower Ordovician and Cambrian epoch (0.7078–0.7091, Burke *et al.* 1982).

Several samples show different strontium isotope characteristics (Fig. 8). LN634-1 and LN631-1 show similar $^{87}Sr/^{86}Sr$ isotopic ratios when compared with adjacent wells, but their high Cl/Br ratios separate them from the cluster of adjacent wells. LG1-4C shows the highest $^{87}Sr/^{86}Sr$ ratio of all our samples, which probably resulted from a stronger exchange with K-bearing minerals. In the case of LG45 and LG47C, the high $^{87}Sr/^{86}Sr$ isotopic ratios may result from another source in the west (Fig. 1A).

DIFFERENT FLOW REGIMES

Based on the chemical and isotopic compositions of the formation waters discussed above, two main flow regimes are proposed:

The western flow regime is represented by wells from Group 2 and consists of mixtures of (i) infiltrating diagenetically altered meteoric waters and (ii) rising diagenetically altered evaporated seawater. Fluids from LG47C and LG45 in the west of Lunnan Fault Block represent a sub-regime based on their higher $^{87}Sr/^{86}Sr$ ratios (>0.711160). Some wells, such as LG15-12 west of the Lunnan Fault Block, cannot be assigned to this sub-regime as cluster characteristics are attributed to Group 2, except for LG47C and LG45. The Lunnan Fault Block was formed by the unification of a NE–SW trending fault and an east–west trending fault in the late Hercynian and Indo-Chinese orogenies (Peng 2004). However, it seems that this activity did not block fluid connectivity between LG15-12 and wells on the east side of Lunnan Fault Block.

The eastern flow regime is represented by wells from Group 1, excluding LG1-4C, LN634-1, and LN631-1, with contributions from diagenetically altered evaporated seawaters and a small proportion of diagenetically altered meteoric waters, and is thus distinguishable from Group 2 wells.

Notably, the two formation-water regimes coincided with the oil and gas occurrences in this region. As reported by Lu *et al.* (2004), two types of oil migrated into the Lunnan Low Uplift from different directions. Heavy oil from the west and light oil from the east resulted in precipitation of asphaltene in the middle zone, which then formed waxy oils. The migration of water seems to reflect the hydrocarbon fluid activities in the Lunnan Low Uplift.

However, some samples do not lie in either of the two regimes. LG1-4C, located in the northeast area, differs from other wells in having the highest $^{87}Sr/^{86}Sr$ ratio of all the samples, indicating that LG1-4C originated from another aquifer toward the northeast (Fig. 1A). LN634-1 and LN631-1 show different chemical compositions from those of adjacent wells. Their Cl, Ca, and Na enrichments (Figs 4 and 5), lower δD and $\delta^{18}O$ values (Fig. 3), and less Mg and SO_4 depletions relative to adjacent wells indicate that both wells may belong to an unknown aquifer connected by faults. Both wells are located close to faults (Fig. 1A).

Several permeability barriers can be defined from the evidence discussed above. Potential barriers separate LG45, LG47C, LG1-4C, LN634-1, and LN631-1 from adjacent wells.

The occurrence of permeability barriers may be a common feature of paleokarst reservoir. With its cave-hole-fissure structure, this type of reservoir is characterized by high permeability and porosity in the same flow regime and by high heterogeneity for the reservoir as a whole. Mixture of different fluids is possible but limited.

EVOLUTION HISTORY

Based on the chemical and isotopic composition of Middle-Lower Ordovician formation waters and the geological setting of the Lunnan Uplift, two hypothetical models of formation-water evolution are proposed as follows (Fig. 9):

Model A (Fig. 9A): During the late Hercynian and Indo-Chinese orogenies, thick sediments of Permian and Carboniferous strata were removed from the top of the Lunnan Uplift. Meteoric waters received external constituents such as Na, Cl, Ca, and ^{87}Sr from interactions with evaporites and K-bearing minerals entering

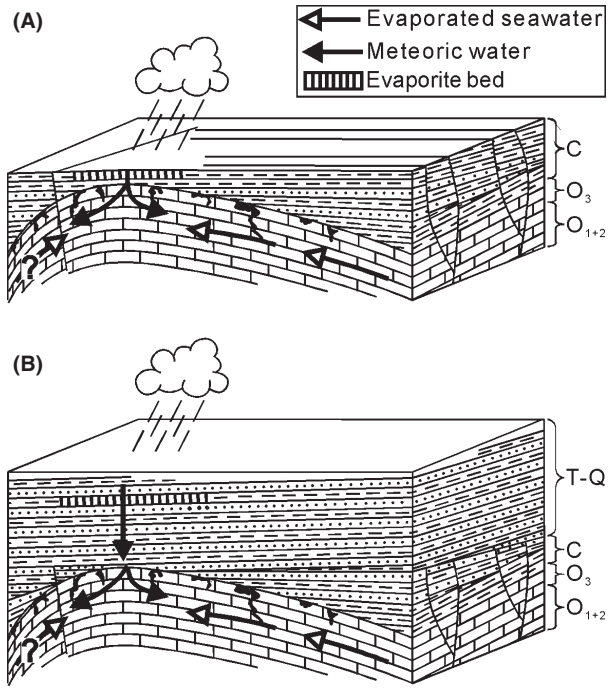

Fig. 9. Two hydrogeological models for the evolution of formation waters. (A) Model A: Meteoric waters dissolving Carboniferous evaporites mixed with evaporated seawaters during late Paleozoic to early Mesozoic period; (B) Model B: Meteoric waters dissolving Paleogene evaporites mixed with evaporated seawaters after Paleogene period. O_{1+2}, O_3, C and T-Q means Middle-Lower Ordovician, Upper Ordovician, Carboniferous strata and strata from Triassic to Quaternary, respectively.

the Ordovician reservoir, and subsequently became mixed with upward-moving diagenetically altered evaporated seawaters from the eastern Cambrian-Lower Ordovician reservoir, which is located in Caohu Sag.

Model B (Fig. 9B): A second meteoric waters infiltration event took place after the deposition of the Paleogene evaporites. Meteoric water leached the evaporites and underlying strata and subsequently mixed with evaporated seawaters from the eastern Caohu Sag to form the present formation water in the Ordovician reservoir.

CONCLUSIONS

Middle-Lower Ordovician formation waters in the Lunnan paleokarst reservoir are a mixture of two fluids: (i) meteoric water that infiltrated into the Ordovician reservoir on the top of the Lunnan Uplift, and (ii) evaporated seawater from the underlying marine strata in Caohu Sag, to the east area of the Lunnan oilfield. Before the fluids entered the current reservoir, diagenetic reactions with minerals occurred. Both waters suffered albitization of plagioclase. Moreover, meteoric water dissolved evaporites and seawater experienced dolomitization. Based on the chemical and isotopic variation of the two fluids, most of the samples can be divided into two groups. Group 1 samples from the east consist of evaporated seawater plus a small proportion of meteoric water, while Group 2 samples from the west are mixtures of meteoric water and evaporated seawater. The different contribution of the two end members explains the spatial distribution of water ions from west to east in this region.

The heterogeneity of the paleokarst reservoir was reflected by compositional variations of formation waters, with several permeability barriers present within the small study region.

ACKNOWLEDGEMENTS

This study was supported by the National Petroleum Project (Grant No. 2011ZX05008-003). We are very grateful to technicians in the State Key Laboratory of Isotope Geochemistry, Guangzhou Institute of Geochemistry, Chinese Academy of Sciences for the strontium isotopic analysis. Thanks go to Prof. Richard Worden, Dr. Ian Billing, and an anonymous reviewer for their critical comments, which greatly improved the quality of the manuscript.

REFERENCES

Barnaby RJ, Oetting GC, Gao GQ (2004) Strontium isotopic signatures of oil-field waters: applications for reservoir characterization. *AAPG Bulletin*, **88**, 1677–704.

Birkle P, Maruri RA (2003) Isotopic indications for the origin of formation water at the Activo Samaria-Sitio Grande oil field, Mexico. *Journal of Geochemical Exploration*, **78–79**, 453–8.

Birkle P, Aragon JJR, Portugal E, Aguilar JLF (2002) Evolution and origin of deep reservoir water at the Activo Luna oil field, Gulf of Mexico, Mexico. *AAPG Bulletin*, **86**, 457–84.

Birkle P, García BM, Milland Padrón CM, Eglington BM (2009) Origin and evolution of formation water at the Jujo-Tecominoacán oil reservoir, Gulf of Mexico. Part 2: Isotopic and field-production evidence for fluid connectivity. *Applied Geochemistry*, **24**, 555–73.

Burke WH, Denison RE, Hetherington EA, Koepnick RB, Nelson HF, Otto JB (1982) Variation of seawater $^{87}Sr/^{86}Sr$ throughout Phanerozoic time. *Geology*, **10**, 516–9.

Cai CF, Franks SG, Aagaard P (2001) Origin and migration of brines from Paleozoic strata in Central Tarim, China: constraints from $^{87}Sr/^{86}Sr$, δD, $\delta^{18}O$ and water chemistry. *Applied Geochemistry*, **16**, 1269–84.

Carothers WW, Kharaka YK (1978) Aliphatic acid anions in oil-field waters: implications for origin of natural gas. *AAPG Bulletin*, **62**, 2441–53.

Chaudhuri S (1978) Strontium isotopic composition of several oilfield brines from Kansas and Colorado. *Geochimica et Cosmochimica Acta*, **42**, 329–31.

Chaudhuri S, Clauer N (1993) Strontium isotopic compositions and potassium and rubidium contents of formation waters in sedimentary basins: clues to the origin of the solutes. *Geochimica et Cosmochimica Acta*, **57**, 429–37.

Chaudhuri S, Broedel V, Clauer N (1987) Strontium isotopic evolution of oil-field waters from carbonate reservoir rocks in

Bindley field, central Kansas, U.S.A. *Geochimica et Cosmochimica Acta*, **51**, 45–53.
Clayton RN, Friedman I, Graf DL, Mayeda TK, Meents WF, Shimp NF (1966) The origin of saline formation waters 1. isotopic composition. *Journal of Geophysical Research*, **71**, 3869–82.
Clescerl LS, Greenberg AE, Eaton AD (1999) *Standard Methods for the Examination of Water and Wastewater*, 20th edn. American Public Health Association, Washington.
Collins AG (1975) *Geochemistry of Oilfield Waters*. Elsevier, New York.
Craig H (1961) Isotopic variations in meteoric waters. *Science*, **133**, 1702–3.
Davis SN (1964) The chemistry of saline waters: discussion. *Ground Water*, **2**, 51.
Davisson ML, Criss RE (1996) Na-Ca-Cl relations in basinal fluids. *Geochimica et Cosmochimica Acta*, **60**, 2743–52.
Egeberg PK, Aagaard P (1989) Origin and evolution of formation waters from oil fields on the Norwegian shelf. *Applied Geochemistry*, **4**, 131–42.
Fan P, Ma BL (1990) *Brief Introduction to Oil and Gas in the Tarim Basin*. Publishing House of Sciences, Beijing (in Chinese).
Fan SF, Zhou ZY (1990) *Thermal History and Petroleum in the Tarim Basin*. Publishing House of Sciences, Beijing (in Chinese).
Fontes JC, Matray JM (1993) Geochemistry and origin of formation brines from the Paris Basin, France 1. brines associated with Triassic salts. *Chemical Geology*, **109**, 149–75.
Gong S, George SC, Volk H, Liu KY, Peng PA (2007) Petroleum charge history in the Lunnan Low Uplift, Tarim Basin, China-Evidence from oil-bearing fluid inclusions. *Organic Geochemistry*, **38**, 1341–55.
Gu JY (1999) Characteristics and evolutional model of karst reservoirs of Lower Ordovician carbonate rocks in Lunnan area of Tarim Basin. *Journal of Palaeogeography*, **1**, 54–60 (in Chinese with English abstract).
Han JF, Wang ZM, Pan WQ, Zhao MJ, Gu QY, Qin SF (2006) Petroleum controlling theory of Lunnan paleohigh and its buried hill pool exploration technology, Tarim Basin. *Petroleum Exploration and Development*, **33**, 448–53 (in Chinese with English abstract).
Hanor JS (1994) Origin of saline fluids in sedimentary basins. In: *Geofluids; Origin, Migration and Evolution of Fluids in Sedimentary Basins*, Vol. **78**. (ed. Parnell J), pp. 151–74. Geological Society, London.
Holser WT (1979) Trace elements and isotopes in evaporites. In: *Marine Minerals: Reviews in Mineralogy*, Vol. **6** (ed. Burns RG), pp. 295–345. Mineralogical Society of America, Washington, DC.
Horita J (2005) Saline waters. In: *Isotopes in the Water Cycle: Past, Present and Future of a Developing Science* (ed. Aggarwal PK, Gat JR, Froehlich KFO), pp. 271–87. Springer, Dordrecht.
Kharaka YK, Hanor JS (2007) Deep fluids in the continents: I. sedimentary basins. In: *Treatise on Geochemistry: Surface and Ground water, Weathering, and Soils*, Vol. **5** (ed. Drever JI), pp. 1–48. Elsevier, Oxford.
Kharaka YK, Thordsen JJ (1992) Stable isotope geochemistry and origin of waters in sedimentary basins. In: *Letter Notes in Earth Science: Isotopic Signatures and Sedimentary Records*, Vol. **43** (eds Clauer N, Chaudhuri S), pp. 411–66. Springer, Berlin.
Li K, Cai C, He H, Jiang L, Cai L, Xiang L, Huang S, Zhang C (2011) Origin of palaeo-waters in the Ordovician carbonates in Tahe oilfield, Tarim Basin: constraints from fluid inclusions and Sr, C and O isotopes. *Geofluids*, **11**, 71–86.
Lico MS, Kharaka YK, Carothers WW, Wright VA (1982) Methods for collection and analysis of geopressured geothermal and oil field waters. United States Geological Survey Water Supply Paper 2194.
Loucks RG (1999) Paleocave carbonate reservoirs; origins, burial-depth modifications, spatial complexity, and reservoir implications. *AAPG Bulletin*, **83**, 1795–834.
Lu H, Jia W, Xiao Z, Sun Y, Peng P (2004) Constraints on the diversity of crude oil types in the Lunnan Oilfield, Tarim Basin, NW China. *Chinese Science Bulletin*, **49**, 19–26.
Machel HG (2001) Bacterial and thermochemical sulfate reduction in diagenetic settings - old and new insights. *Sedimentary Geology*, **140**, 143–75.
Mazzullo SJ, Chilingarian GV (1996) Hydrocarbon reservoirs in karsted carbonate rocks. In: *Developments in Petroleum Sciences: Carbonate Reservoir Characterization: A Geologic - Engineering Analysis*, Vol. **44** (eds Chilingarian GV, Mazzullo SJ, Rieke HH), pp. 797–865. Elsevier, Amsterdam.
McCaffrey MA, Lazar B, Holland HD (1987) The evaporation path of seawater and the coprecipitation of Br^- and K^+ with halite. *Journal of Sedimentary Research*, **57**, 928–37.
Mook WG (2000) *Environmental Isotopes in the Hydrologic Cycle: Principles and Applications, Vol. II: Atmospheric water*. IAEA, Paris.
Pang W, Shi HX (2008) The paleo-karst feature of Ordovician carbonate rocks in Lunnan Area. *Xinjiang Petroleum Geology*, **29**, 37–40 (in Chinese with English abstract).
Pang W, Jiang TW, Zheng JM, Shi HX (2007) Characteristics of the Ordovician buried hill reservoirs in Tahe-Lunnan oil area. *Oil & Gas Geology*, **28**, 762–7. (in Chinese with English abstract).
Peng PA (2004) Research on source, accumulation processes of petroleum in the Lunnan area. Internal report. Guangzhou Institute of Geochemistry, Chinese Academy of Sciences (in Chinese).
Rittenhouse G (1967) Bromine in oil-field waters and its use in determining possibilities of origin of these waters. *AAPG Bulletin*, **51**, 2430–40.
Ruan Z, Yu BS, Zhu JF (2009) Research on the characteristics of Ordovician reef-flat reservoirs in the Tarim Basin. *Geoscience*, **23**, 691–8 (in Chinese with English abstract).
Russell CW, Cowart JB, Russell GS (1988) Strontium isotopes in brines and associated rocks from Cretaceous strata in the Mississippi Salt Dome Basin (southeastern Mississippi, U.S.A.). *Chemical Geology*, **74**, 153–71.
Sofer Z, Gat JR (1972) Activities and concentrations of oxygen-18 in concentrated aqueous salt solutions: analytical and geophysical implications. *Earth and Planetary Science Letters*, **15**, 232–8.
Stoessell RK, Carpenter AB (1986) Stoichiometric saturation tests of $NaCl_{1-X}Br_X$ and $KCl_{1-X}Br_X$. *Geochimica et Cosmochimica Acta*, **50**, 1465–74.
Stueber AM, Walter LM (1991) Origin and chemical evolution of formation waters from Silurian-Devonian strata in the Illinois Basin, USA. *Geochimica et Cosmochimica Acta*, **55**, 309–25.
Stueber AM, Walter LM, Huston TJ, Pushkar P (1993) Formation waters from Mississippian-Pennsylvanian reservoirs, Illinois Basin, USA: chemical and isotopic constraints on evolution and migration. *Geochimica et Cosmochimica Acta*, **57**, 763–84.
Stueber AM, Saller AH, Ishida H (1998) Origin, migration, and mixing of brines in the Permian Basin: geochemical evidence

from the eastern Central Basin Platform, Texas. *AAPG Bulletin*, **82**, 1652–72.

Tang LJ, Jin ZJ, Jia CZ, Pi XJ, Chen SP (2004) The relationship between multiple salt structures and petroleum accumulation in the Tarim Basin. *Science in China Series D-Earth Sciences*, **34I**, 89–97 (in Chinese).

Wang CG (2001) Characteristics of clastic reservoirs in the Tarim Basin. *Petroleum Geology & Experiment*, **23**, 62–6 (in Chinese with English abstract).

Wang XM, Zhang SC (2008) Distribution and genesis of natural gas in the Lunnan area. *Oil & Gas Geology*, **29**, 204–9 (in Chinese with English abstract).

Wang TG, Li SM, Zhang SC (2004) Oil migration in Lunnan region, Tarim Basin, China based on the pyrrolic nitrogen compound distribution. *Journal of Petroleum Science and Engineering*, **41**, 123–34.

Worden RH (1996) Controls on halogen concentrations in sedimentary formation waters. *Mineralogical Magazine*, **60**, 259–74.

Worden RH, Smalley PC, Oxtoby NH (1995) Gas scouring by thermochemical sulfate reduction at 140°C. *AAPG Bulletin*, **79**, 854–63.

Xiao XM, Hu ZL, Jin YB, Song ZG (2005) Hydrocarbon source rocks and generation history in the Lunnan oilfield area, Northern Tarim Basin (NW China). *Journal of Petroleum Geology*, **28**, 319–33.

Xu Z, Ai L (2011) Sedimentary facies features of Carboniferous sand-mud stone in Lunnan paleo-uplift, the northern Tarim Basin. *Journal of Xi'an Shiyou University (Natural Science Edition)*, **26**, 31–8. (in Chinese with English abstract).

Yang HJ, Han JF (2007) Characterization and controlling factors of Lunnan multiple oil and gas accumulation in the Tarim Basin. *Science in China Series D-Earth Sciences*, **37II**, 53–62 (in Chinese).

Yang F, Sun YS (1999) Reservoir characteristics of the major gas reservoirs in the Tarim Basin. *Natural gas industry*, **19**, 43–9 (in Chinese with English abstract).

Yun L, Zhai XX (2008) Discussion on characteristics of the Cambrian reservoirs and hydrocarbon accumulation in Well Tashen-1, Tarim Basin. *Oil & Gas Geology*, **29**, 726–32 (in Chinese with English abstract).

Zhang SC, Hanson AD, Moldowan JM, Graham SA, Liang DG, Chang E, Fago F (2000) Paleozoic oil-source rock correlations in the Tarim Basin, NW China. *Organic Geochemistry*, **31**, 273–86.

Zhou JY, Han YY, Lin ZM (1999) Sedimentary evolution and salt-forming mechanism in lower Carboniferous salt-bearing series, northern Tarim Basin. *Xinjiang Petroleum Geology*, **20**, 244–7 (in Chinese with English abstract).